Journal of Magnetism and Magnetic Materials 544 (2022) 168682

Contents lists available at ScienceDirect

Journal of Magnetism and Magnetic Materials

journal homepage: www.elsevier.com/locate/jmmm

Magnetic properties of Co-Tb alloy films and Tb/Co multilayers as a function of concentration and thickness

Łukasz Frąckowiak [a,*], Feliks Stobiecki [a], Maciej Urbaniak [a], Michał Matczak [b], Gabriel David Chaves-O`Flynn [a], Mikołaj Bilski [c], Andreas Glenz [d], Piotr Kuświk [a]

[a] Institute of Molecular Physics, Polish Academy of Sciences, Poznań, Poland
[b] Faculty of Physics, University of Białystok, Białystok, Poland
[c] Institute of Applied Mechanics, Poznań University of Technology, Poznań, Poland
[d] Science & Research Division, PREVAC sp. z o.o., Rogów, Poland

ARTICLE INFO

Keywords:
Co-sputtering
Ferrimagnetic films
Compensation composition
Thin films
Multilayers

ABSTRACT

Deposition of alloy films with a well-controlled concentration gradient obtained by co-sputtering from two magnetron sources is studied experimentally and compared with numerical calculations. This method was used together with a linearly moving shutter to fabricate sperimagnetic Co-Tb alloy films with mutually orthogonal concentration and thickness gradients. Using magnetooptical measurements it was demonstrated that, for thicknesses below 10 nm, the compensation concentration (c_{comp}) shifts towards higher Tb content as the thickness of the Co-Tb film is reduced. Results for Co-Tb alloy films are compared with those for $(Tb/Co)_{RN}$ multilayers with various repetition numbers (RN). For both sample types, the c_{comp} decreases in a similar way with increasing total film thickness. Thus, the decrease of c_{comp} with increasing total thickness (either of alloy films or of multilayers) can be considered a universal behavior.

1. Introduction

Studies aimed at developing new thin film materials and optimizing their composition and thickness for application in fields such as e.g. electronics, information technologies, photonics, photovoltaics, spintronics, and magnonics have been carried out in numerous laboratories worldwide for several decades now. Among the various methods of producing complex thin film systems, both in industrial and laboratory settings, magnetron sputtering is among the most frequently used [1]. The possibility to create films with gradients of thickness [2–7] and/or concentration [8–20] (in some publication these methods are named as combinatorial depositions) significantly facilitates the optimization of thin films or layered systems. However, an important condition for the use of this type of films in material research is the possibility to test their properties locally.

This paper examines the magnetic properties of sperimagnetic Co-Tb alloy films [21–26] with a Tb concentration (c^{Tb}) gradient parallel to one edge of the rectangular substrate and a thickness ($t^{Co\text{-}Tb}$) gradient perpendicular to that edge. We examine their properties as a function of c^{Tb} and $t^{Co\text{-}Tb}$ using hysteresis loops measured with magneto-optical Kerr effect. The films were deposited by co-sputtering from two magnetron sources, to obtain the c^{Tb} gradient, while the use of a shutter moving in the direction perpendicular to the c^{Tb} gradient provided a $t^{Co–Tb}$ gradient.

Co-Tb films were selected for these experiments because their magnetic properties, similarly to other ferrimagnetic or sperimagnetic alloys, depend strongly on c^{Tb}. This behavior is a consequence of the antiferromagnetic interaction between the transition metal (Co) and rare earth (Tb) subsystems that induces a reduction of the effective magnetization. As a result, at a specific, temperature-dependent concentration (c_{comp}), the magnetizations of both subsystems compensate, which is manifested by zero effective magnetization and a divergence of the coercive field ($H_C(c^{Tb})$) [4,27]. Moreover, though Co-Tb films [21,28–30] show well-known changes in magnetic properties with film thickness, the thickness vs c_{comp} dependence for this type of sperimagnetic film is unknown. Considering that magnetic properties of sperimagnetic/ferrimagnetic films in the vicinity of c_{comp} are particularly attractive for applications [4,30–41], we focus on that dependence for Tb-Co alloy films as well as for Tb/Co multilayers. For sperimagnetic Fe-Tb alloy films, Hebler *et al.* [30] found that c_{comp} increases with

* Corresponding author at: ul. Mariana Smoluchowskiego 17, 60-179 Poznań, Poland.
E-mail address: lukasz.frackowiak@ifmpan.poznan.pl (Ł. Frąckowiak).

https://doi.org/10.1016/j.jmmm.2021.168682
Received 2 July 2021; Received in revised form 7 September 2021; Accepted 28 September 2021
Available online 22 October 2021

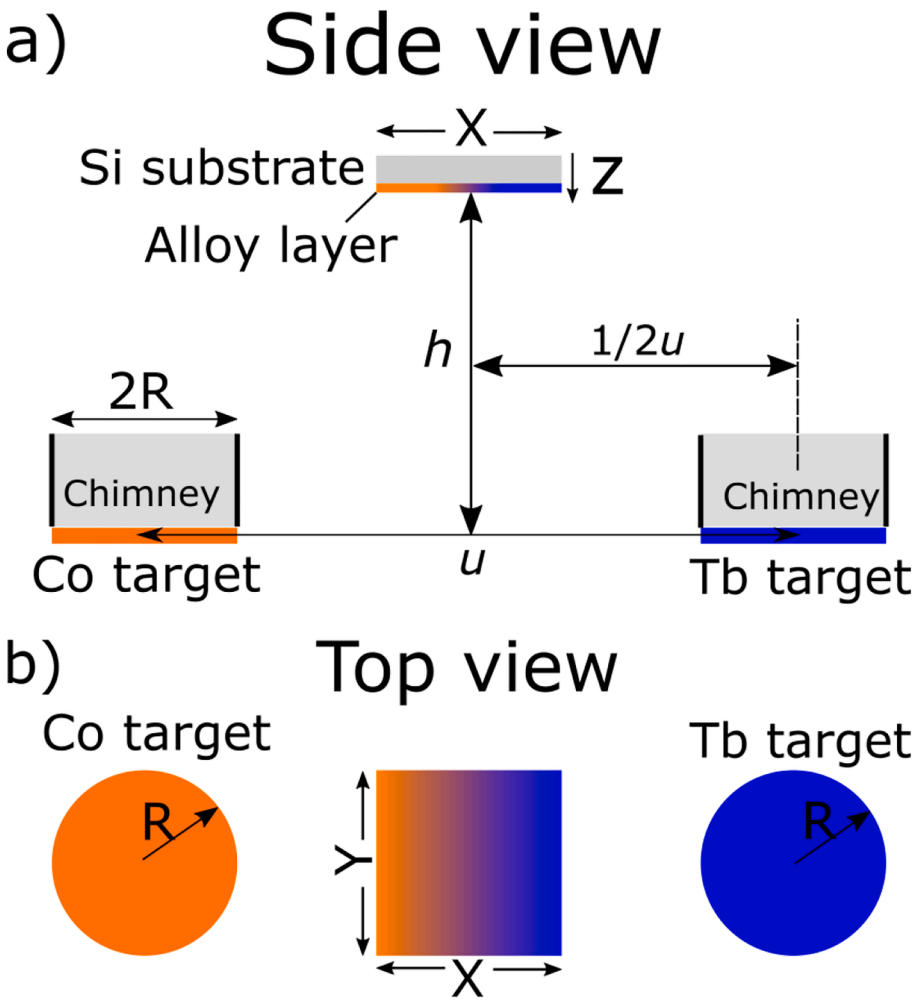

Fig. 1. Schematic view of targets and substrate positions during the co-sputtering deposition of Co-Tb alloy films indicating relevant geometric parameters: R – radius of the target, u – distance between targets, h – distance between target and substrate planes. (a) Side view, (b) top view. Blue and orange colors represent Co and Tb, respectively.

decreasing t^{FeTb}. The physical origin of these changes was attributed to the distribution of Tb magnetic moments (fanning cone) related to morphology and microstructure in the first 20–30 nm of amorphous Fe-Tb films [30]. More collinearly aligned Tb moments along the out-of-plane direction with film thickness are equivalent to increasing Tb concentrations; and therefore, are responsible for decreases of c_{comp} with t^{FeTb}. Note that in the case of Tb-Fe, the Fe also shows a fanning cone that reduces the out of plane component from its sublattice. Considering that the Co fanning cone in Tb-Co is strongly reduced in comparison to that of Fe in Fe-Tb, our studies of c_{comp} vs Co-Tb thickness may support this interpretation.

An additional argument for choosing this material is that, in recent years, interest in ferrimagnetic/sperimagnetic RE-TM films with bulk perpendicular magnetic anisotropy (PMA) has experienced a renaissance owing to properties attractive for new applications, such as: tunable perpendicular exchange coupling [4,31,32], tunable amplitude of the magnetoresistance signal [33], all-optical switching [30,34], fast domain wall propagation [35,36], manipulation of domain walls using thermal gradients [37], current-induced magnetization switching with spin–orbit torque effect [38,39,42], and creation and propagation of skyrmions [36]. Moreover, the ability to control in-plane concentration gradients in ferrimagnetic Gd-Co films [40] allows to study magnetization reversal in the vicinity of c_{comp} at fixed temperatures, as well as laser-induced spin dynamics close to the angular momentum compensation point [41].

The paper is organized as follows: we begin with a description of the conditions for deposition of the films, the measurement of their composition, and the characterization of their magnetic properties. The second part introduces a model used to calculate thickness distribution and element concentration of alloy films produced by magnetron co-sputtering. The third part gives a comparison between these calculation results with measurements of concentration distribution. The final part provides a summary of magnetic properties of Co–Tb alloy films as functions of c^{Tb} and t^{Co-Tb}, which are then compared with $(Tb/Co)_{RN}$ (RN–repetition number) multilayers, indicating that decrease of c_{comp} with total film thickness is similar for both kind of samples.

2. Experimental

The deposition process was carried out using magnetron sputtering (MS) system (detailed description of the system is given in supplementary materials) at room temperature (RT) in an Ar (5 N) atmosphere of $p_{Ar} \cong 1.5 \times 10^{-3}$ mbar partial pressure (base pressure $p_{\infty} \leq 5 \times 10^{-8}$ mbar). Fig. 1 presents a schematic view of target and substrate relative positions during co-sputtering deposition. The substrates were naturally oxidized Si(1 0 0) wafers with dimensions of 20 × 20 mm^2, covered with a buffer layer of Ti-4 nm/Au-30 nm. This type of buffer layer was used for Tb/Co multilayers that exhibit PMA and has been described elsewhere [4,5,7]. The buffer layer was deposited immediately before the deposition of Co-Tb layers, which were protected against oxidation with

Table 1
Deposition conditions for Co-Tb alloy films and Tb/Co multilayers.

The structure	Co target power	Tb target power
Co-Tb alloy film deposited at $h = 97$ mm	49 W dc	21 W rf
Co-Tb alloy film deposited at $h = 147$ mm	47 W dc	23 W rf
Co-Tb wedge shaped alloy film $0 \leq t^{Co\text{-}Tb} \leq 10$ nm, $h = 97$ mm	36 W dc	44 W rf
Co-Tb wedge shaped alloy film $0 \leq t^{Co\text{-}Tb} \leq 30$ nm, $h = 97$ mm	36 W dc	44 W rf
Tb/Co multilayers deposited at $h = 60$ mm	35 W dc	8 W rf

an Au-5 nm layer.

A quartz balance with an 8 mm diameter active area was mounted on the substrate holder placed in the co-sputtering position (the location of the sensor center corresponded to the location of the substrate center during the deposition of the Co-Tb alloy layer) to determine deposition rates for Tb and Co as functions of power applied to the magnetron source ($R^{Tb}_{sput}(P)$ and $R^{Co}_{sput}(P)$) (Fig. S2) at $h = 97$ mm and $h = 147$ mm (meaning of the h parameter is explained in Fig. 1).

For studies of concentration profile in the co-sputtered Co-Tb alloy films, two Ti-4 nm/Au-30 nm/$Co_{100-x}Tb_x$ - $t^{Co\text{-}Tb}$/Au-5 nm ($x = c^{Tb}$) samples were deposited at $h = 97$ mm and $h = 147$ mm. The values of R^{Co}_{sput} and R^{Tb}_{sput}, for a given h depending on P (Fig. S2 and Table 1), and the deposition time (s_t), were chosen so as to obtain the thickness of the Co-Tb layer $t^{Co\text{-}Tb} \approx 30$ nm and Tb concentration $c^{Tb} \approx 22$ at.% at the center of the substrate. The parameters of the deposition process are determined with the following assumptions: (i) the deposition rates R^{Co}_{sput} and R^{Tb}_{sput} (Fig. S2) represent values at the center of the substrate, (ii) the $t^{Co–Tb}$ is the sum of Co and Tb partial thicknesses ($t^{Co} + t^{Tb}$). Values for c^{Tb} can then be obtained from t^{Co}, t^{Tb}, and the molar volume of each element $V^{Tb(Co)}$ [43]:

$$c^{Tb} = \frac{\frac{t^{Tb}}{V^{Tb}}}{\frac{t^{Tb}}{V^{Tb}} + \frac{t^{Co}}{V^{Co}}} \quad (1)$$

To study the magnetic properties of Co-Tb alloy films as functions of c^{Tb} and $t^{Co\text{-}Tb}$, the following two structures were deposited: Ti-4 nm/Au-30 nm/$Co_{100-x}Tb_x$-wedge-0–10 nm/Au-5 nm and Ti-4 nm/Au-30 nm/$Co_{100-x}Tb_x$-wedge-0–30 nm/Au-5 nm. The magnetic properties of these Co-Tb alloy films were compared with those of the Ti-4 nm/Au-30 nm/(Tb-wedge-0–2 nm/ Co–0.66 nm)$_{RN}$ multilayers. Note that similar multilayers with RN = 6 were studied in our earlier work [4]. The deposition conditions for Co-Tb alloy films and Tb/Co multilayers are given in Table 1. The buffer (Ti/Au) and cover (Au) layers for all the samples were deposited at $h = 60$ nm using dc 50 W and rf 20 W power supply for Ti and Au, respectively.

The c^{Tb} profile was measured using X-ray microanalysis on a FEI Nova Nano SEM scanning electron microscope equipped with a Bruker EDS detector. The energy of primary electron beam was 30 keV. A c^{Tb} distribution map was obtained for the entire sample averaging over 0.5 × 0.5 mm^2 areas that correspond to the cross section of the scanning beam.

The magnetic properties of alloys and multilayers were investigated using polar magneto-optical Kerr effect (P-MOKE). The maximum value of the external magnetic field was ± 15 kOe. A 655 nm wavelength laser with a spot size of 0.2 mm was used in the P-MOKE magnetometer. The changes in magnetic properties as functions of Tb concentration and/or Co-Tb thickness were investigated by moving the sample relative to a stationary laser beam.

3. Numerical calculation of thickness and concentration profiles for alloy films deposited by two-target co-sputtering

The determination of concentration profiles for alloy films deposited by co-sputtering was the subject of some previous works (e.g., [9,11,13,44–46]). Here, we will introduce a model that assumes a cosine distribution for the atoms emitted from a point source under UHV conditions [47], and predicts numerical values for the thickness of given materialat point k of the substrate plane (t_k) (Fig. 2). For co-sputtering from Tb and Co targets, the set of $\{t_k^{Tb}, t_k^{Co}\}$ values, for all elementary areas of the substrate, allows to create distribution maps of t^{Co}, t^{Tb}, $t^{Co–Tb}$, and c^{Tb}.

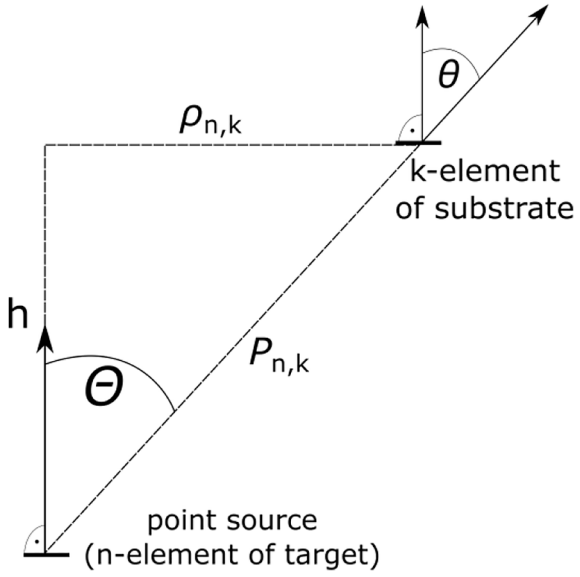

Fig. 2. Schematic representation of geometrical parameters needed to calculate lateral concentration profiles of co-sputtered alloy films.

To perform numerical calculations, the target and substrate surfaces have been divided into N and K squares, respectively. Emission from each element of the target is calculated using its midpoint coordinates to determine the angle relevant for the Knudsen's cosine law (Fig. 2) [45,47]. To incorporate real effects that occur at the targets during sputtering it is worth considering two possible cases. The first case assumes that all points of the target contribute to the growth of the sample; in this case, each target point $A_n = (x_n, y_n, 0)$ is considered to contribute to sample growth:

$$\sqrt{(x_n - x_0)^2 + (y_n - y_0)^2} \leqslant R, \quad (2)$$

where (x_0, y_0) is the position of the target's center. However, during deposition with magnetron sources, the sputtering of the target takes place mainly within an annular area (Fig. S3). To account for this phenomenon, more stringent conditions are considered in a second case where only points of the target located within $R_1 = 10$ mm and $R_2 = 20$ mm radii are assumed to contribute to sample growth. In this case, for each n–th element of the target the following relationship must be satisfied:

$$R_1 \leqslant \sqrt{(x_n - x_0)^2 + (y_n - y_0)^2} \leqslant R_2. \quad (3)$$

We will refer to these two cases as "disk" and "annulus" targets.

The t_k at the k–th element of the substrate, denoted as $B_k = (x_k, y_k, h)$, was determined using the equation:

$$t_k = s_t G(x_k, y_k)\varepsilon, \quad (4)$$

where: s_t is the deposition time, ε is the source yield (i.e. the total volume of the sputtered material per unit time), $G(x_k,y_k)$ is the "deposition profile by unit area" that describes the distribution of deposited material as a function of position on the substrate. The value of this coefficient is given by [45,48]:

$$G(x_k, y_k) = \sum_n^N cos\Theta_{n,k} \cdot cos\theta_{n,k} \cdot \frac{1}{P_{n,k}^2}, \text{ where} \quad (5)$$

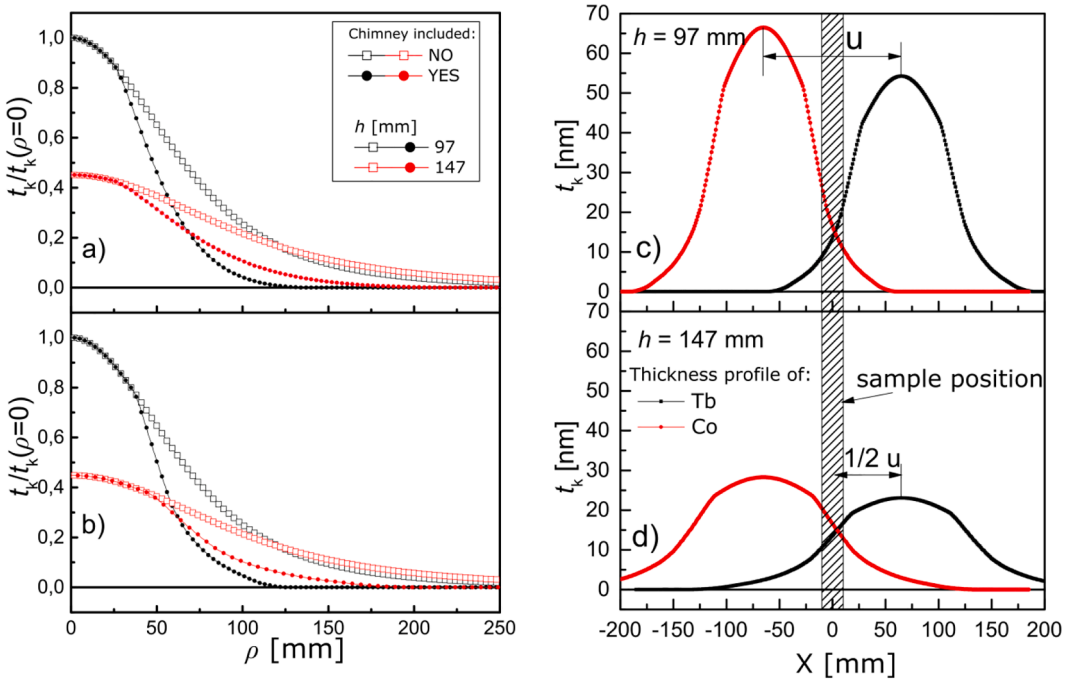

Fig. 3. Normalized (with respect to value at $\rho = 0$: $t_k(\rho)/t_k(\rho = 0)$) thickness profiles as a function of distance from the target axis), calculated for the deposition from a single target at $h = 97$ mm and $h = 147$ mm, with and without the chimneys for the (a) disk and (b) annulus target. A deposition profile $G(\rho)$ corresponding to thickness profile is given in supplementary materials Fig.S5. Calculated exemplary thickness profiles of Tb (black) and Co (red) deposited from annulus targets for (c) $h = 97$ mm and (d) $h = 147$ mm as a function of the location relative to the center of the substrate X (for Y = 0). To calculate $t^{Co-Tb} = 30$ nm and $c^{Tb} = 22$ at.% in the sample center, we took the yield of the sputtering processes to be (c) $\varepsilon_{Tb} = 3.71{\cdot}10^{-6}$ mm^3/s, $\varepsilon_{Co} = 4.55{\cdot}10^{-6}$ mm^3/s for $h = 97$ mm and (d) $\varepsilon_{Tb} = 3.55{\cdot}10^{-6}$ mm^3/s, $\varepsilon_{Co} = 4.36{\cdot}10^{-6}$ mm^3/s for $h = 147$ mm and deposition time $s_t = 150$ s. The hatched area corresponds to the region occupied by the substrate.

$$cos\Theta_{n,k} = cos\theta_{n,k} = \frac{h}{\sqrt{h^2 + \rho_{n,k}^2}}, \tag{5.1}$$

$$P_{n,k} = \sqrt{h^2 + \rho_{n,k}^2}, \tag{5.2}$$

$$\rho_{n,k} = \sqrt{(x_k - x_n)^2 + (y_k - y_n)^2}. \tag{5.3}$$

The magnetron sources are equipped with chimneys (Fig. 1). Due to their presence, some of the material sputtered from the target is deposited on the inner surfaces of the chimney. Thus, some regions of the target do not contribute to the growth of the film at a given point k. We account for this effect by rejecting each element of the target for which the line connecting points A_n (target) and B_k (substrate) intersects the surface of the chimney (see Suplementary Materials for more detail information). The values of t_k for Tb (t_k^{Tb}) and Co (t_k^{Co}) determined from formulas (3–5) and considering condition (2, 3) allow to calculate, for each k–element, the concentration of Tb (c_k^{Tb}) using an equation analogous to Eq. (1) [43].

Due to the axial symmetry of our targets, we can substitute the (x_k, y_k) position parameter with a radial parameter, ρ, which denotes the distance between point B_k and the target axis ($x_n = x_0$, $y_n = y_0$), as follows:

$$\rho = \sqrt{(x_k - x_0)^2 + (y_k - y_0)^2}. \tag{6}$$

Fig. 3 shows numerically obtained profiles of normalized thickness $t_k(\rho)/t_k(\rho = 0)$ in single target sputtering with the substrate at two different heights ($h = 97$ mm and $h = 147$ mm), for disk and annulus targets, with and without chimney. The $G(\rho)$ dependence corresponding to thickness profile presented in Fig. 3 is given in supplementary material as Fig. S5. The thickness profiles depend only slightly on considerations about the target's shape, whereas a change in height or the chimney's insertion have a significant impact on it. Based on the actual conditions of the experiment, subsequent discussion will focus on calculations for annular targets with chimneys. We will also limit the discussion to $h = 97$ mm because a wider range of c^{Tb} values can be obtained at this height, as will be shown later (results for $h = 147$ mm and disk target are provided as Supplementary Materials).

Fig. 3c,d show profiles of partial thickness for Tb ($t_k^{Tb}(X)$) and Co ($t_k^{Co}(X)$) as functions of distance to the substrate center, X, in the configuration of Fig. 1 (note that the point at X = 0 and Y = 0 corresponds to the substrate center $\rho_{Tb} = 65$ mm). The values t_k^{Co} and t_k^{Tb} at various positions on the substrate were used to calculate two-dimensional maps for t^{Co-Tb} and c^{Tb} (Fig. 4 a,b and Fig. S6, Fig. S7).

To test the model, the c^{Tb} profile was measured for Co-Tb films deposited at two different heights h. The composition was measured every 1 mm along the X axis and every 3 mm along the Y axis. The $c^{Tb}(X, Y)$ distribution map for $h = 97$ mm is shown in Fig. 4c; and for $h = 147$ mm, in Fig. S8a. Fig. 4d and Fig. S8b show comparisons between experimental measurements and numerical calculations which are in excellent agreement. They also indicate that, despite slight changes of t^{Co-Tb} along the Y axis for a given X, c^{Tb} appears to be independent of Y.

4. Magnetic properties of Co-Tb films as a function of concentration and thickness

Maps of H_C distribution in Co-Tb alloy films were obtained from local PMOKE hysteresis loop measurements at RT (Fig. 5a and Fig. S9a). H_C is very sensitive to changes of c^{Tb} near c_{comp}, [31,33,34,49] and diverges as c^{Tb} approaches c_{comp} from either the Co+ or the Tb+ sides (Fig. 5a,b and Fig. S9a,b). Near c_{comp}, there is a range of c^{Tb} values which is not experimentally accessible because it requires field magnitudes larger than those experimentally available in our set-up (~15 kOe). This experimentally inaccessible area is visible as a white stripe in Fig. 5a (and Fig. S9a). There is a slight deviation from the Y axis for lines of constant H_C and for the compensation point region (Fig. 5a) which we attribute to misalignments between the substrate and the sample holder

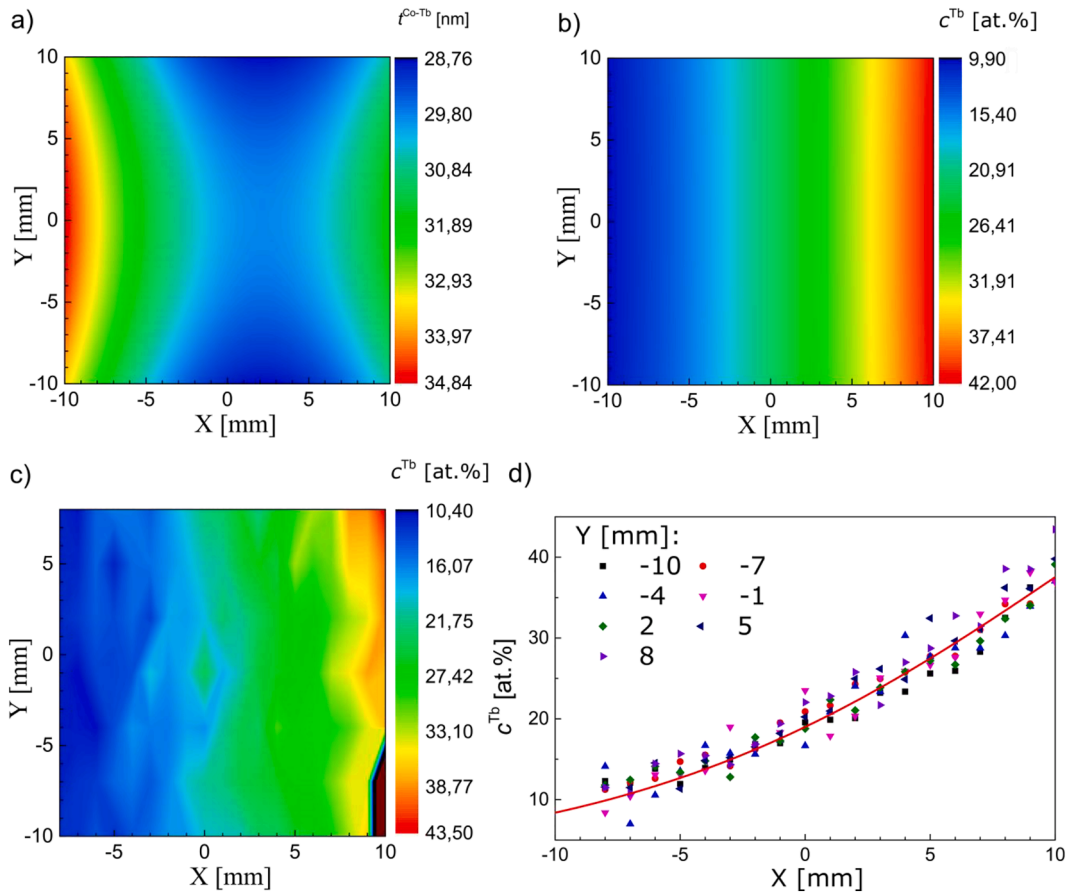

Fig. 4. (a) Calculated maps of thickness (t^{Co-Tb}) and (b) concentration (c^{Tb}) profiles for Co-Tb alloy films deposited at $h = 97$ mm, as a function of the position relative to the substrate's center. (c) Map of concentration profile determined from X-ray microanalysis. (d) c^{Tb}(X) – comparison of the calculated values at Y = 0 mm (red line) and experimental results for a multiples values of Y.

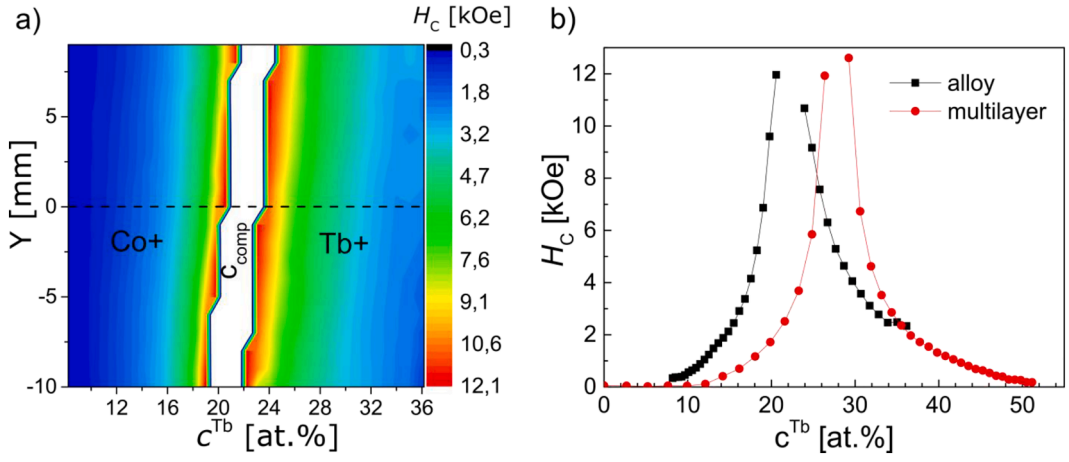

Fig. 5. (a) Map of coercive field (H_C) determined from magnetooptical hysteresis loops for the Co-Tb alloy film deposited at $h = 97$ mm. (b) $H_C(c^{Tb})$ for the alloy film and for the (Tb-wedge-0–2 nm/ Co-0.66 nm)$_6$ multilayer

during measurement and/or deposition.

Since c^{Tb} does not change with Y, and t^{Co-Tb} does it only slightly (Fig. 4a,b, Fig. S6 and Fig. S7), all the relevant information contained in this map can be extracted from a horizontal cut along Y = 0 showing H_C as a function of c^{Tb} alone (Fig. 5b and Fig. S9b). For comparison, $H_C(c^{Tb})$ values for (Tb–wedge–0–2 nm/Co-0.66 nm)$_6$ multilayer are also shown.

It is worth noticing that the hysteresis loop shapes are close to ideal rectangles for the whole concentration range (except $c^{Tb} \leq 13$ at.%) i.e., $\varphi_R/\varphi_S \approx 1$ where φ_R and φ_S denote Kerr signal in remanence and saturation, respectively (Fig. S10a,b). For alloy films, c_{comp} is about 21–22 at.%, which agrees very well with literature reports [31,33,34]; however, this value is clearly lower than the value for multilayers, which is about 27 at.%. It should be noted here that the thickness of the (Tb/Co)$_6$ multilayer at the compensation point is about 9 nm, which is less than one third of the alloy film's thickness.

Two additional alloy films were co-sputtered to investigate the

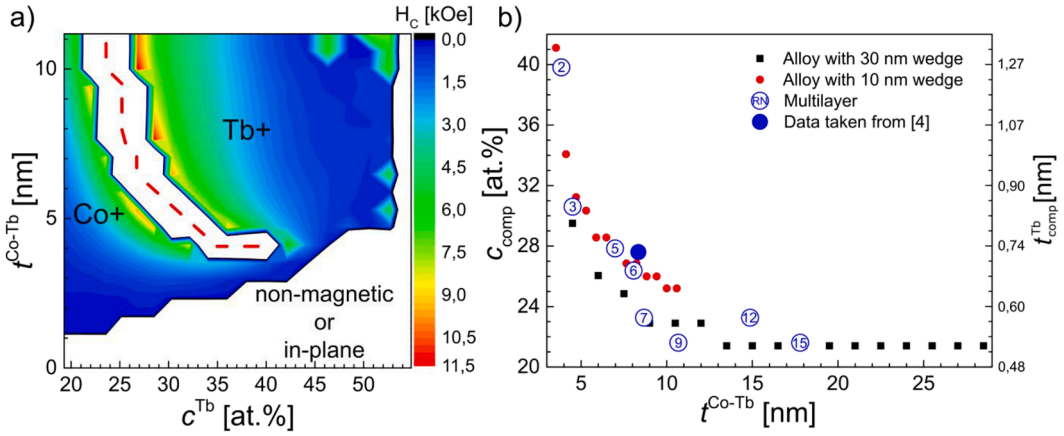

Fig. 6. (a) Map of coercive fields (H_C) dependence on Tb concentration (c^{Tb}) and film thickness ($t^{Co\text{-}Tb}$) for the 10 nm wedge shaped Co-Tb film with c^{Tb} gradient perpendicular to $t^{Co\text{-}Tb}$ gradient [red dashed line corresponds to the compensation composition (c_{comp})]. (b) $c_{comp}(t^{Co\text{-}Tb})$ determined for two alloy films with different range of $t^{Co\text{-}Tb}$ changes and for eight (Tb-wedge-0–2 nm/Co-0.66 nm)$_{RN}$ (RN = 2, 3, 5, 6, 7, 9, 12, and 15) multilayers (for multilayers $t^{Co\text{-}Tb}$ denote total thickness at c_{comp}). For comparison we also show data for RN = 6 taken from Ref. [4]. For Tb/Co multilayers right axis indicate $t^{Tb}{}_{comp}$ i.e., Tb thickness corresponding to c_{comp}.

discrepancy of c_{comp} values between multilayer and alloy, and to determine whether it is due to changes of the total thickness, or whether it has a morphological origin. These films are grown with an additional $t^{Co\text{-}Tb}$ gradient that is perpendicular to the original c^{Tb} gradient obtained by co-sputtering and is achievable by controlling the shutter's motion. This process establishes a natural choice of coordinates in which c^{Tb} and $t^{Co\text{-}Tb}$ are associated with the X and Y coordinates of points in the sample's plane. The deposition parameters of these films were chosen so that their composition changed within the $19 \le c^{Tb} \le 55$ at.% range; and the thickness in the ranges $0 \le t^{Co\text{-}Tb} \le 10$ nm and $0 \le t^{Co\text{-}Tb} \le 30$ nm for the first and second sample, respectively (Table 1). For the first sample, a map of H_C as a function of c^{Tb} and $t^{Co\text{-}Tb}$ is shown in Fig. 6a. The white curved area located in the left upper part corresponds to the compensation region (similar to Fig. 5a). However, the white area in the bottom and right part corresponds to either nonmagnetic behavior or to the in-plane anisotropy. It is worth noticing that, in contrast to (Co–Tb/Ti)$_{RN}$ multilayers [21,29], our Co-Tb films exhibit PMA for $10 \le c^{Tb} \le 50$ at.% and $t^{Co\text{–}Tb} \ge 5$ nm.

Fig. 6b shows c_{comp} vs. $t^{Co\text{-}Tb}$ for our two Co-Tb alloy films and eight (Tb-wedge-0–2 nm/ Co–0.66 nm)$_{RN}$ multilayers with RN equal to 2, 3, 5, 6, 7, 9, 12, and 15 (for RN = 6 we also show data taken from Ref. [4]). It is worth to notice that, according to [50], the Tb/Co multilayers behave like alloy films for sublayer thicknesses smaller than 1 nm. Except for the point corresponding to RN = 2 ($c_{comp} \approx 40$ at.%, $t^{Tb} \approx 1.26$ nm) all other experimental points correspond to $t^{Tb} < 1$ nm and $t^{Co} < 1$ nm. For both systems we found that the c_{comp} decreases with an increase of $t^{Co\text{-}Tb}$ and $t^{Tb/Co}$. This behavior is similar to that presented in Fig. 3c of Ref. [30], for Fe-Tb sperimagnetic alloy films. Therefore, it can be assumed that the physical mechanism is the same in both cases and results from short-range ordering of a transition metal with the Tb in the sperimagnetic alloy films. This leads to a broad distribution of orientations of magnetic moments of Fe and Tb in the Fe-Tb alloy (see Fig. 1 in [30]). However, in the case of Tb-Co where the exchange interaction between Co's is stronger, the wide angular distribution is present only in Tb [26]. This different distribution explains why the $c_{comp}(t^{Co\text{-}Tb})$ relationship for Co-Tb alloys saturates at smaller thickness than for Fe-Tb alloys [30]. A comparison of the results for alloy films with different $t^{Co\text{–}Tb}$ ranges, Fig. 6b, manifests very good repeatability of the deposition process. The c_{comp} values determined for eight (Tb-wedge-0–2 nm/Co-0.66 nm)$_{RN}$ multilayers deposited in various processes are much more scattered, however the experimental values of $c_{comp}(t^{Co\text{-}Tb})$ show the same behavior as seen for alloy films. Thus, decrease of c_{comp} with the total thickness of alloy films or multilayers can be seen as a universal behavior.

5. Conclusion

This paper shows that properties of alloys as functions of composition and thickness can be determined from a single sample that consists of a wedge-shaped alloy film deposited with co-sputtering from separate targets. We focus on the magnetic properties of Co-Tb alloys as a representative example. This work also presents a numerical procedure to calculate concentration profiles of deposited films in two steps: the first step provides the lateral dependence of each element's partial thickness; based on these results, the second step yields thickness and concentrations for any point of the substrate. The model was validated with local composition and magnetic measurements from X-ray microanalysis and the magneto-optical magnetometry. Magnetic measurements of Co-Tb films with mutually orthogonal concentration and thickness gradients showed that, for thicknesses below 10 nm, the compensation concentration shifts towards higher concentration of Tb as the total film thickness is reduced. This behavior, important for a broad range of applications, is of the same nature for Co-Tb alloy films and Tb/Co multilayers.

CRediT authorship contribution statement

Łukasz Frąckowiak: Conceptualization, Methodology, Software, Validation, Formal analysis, Investigation, Visualization, Writing – original draft, Writing – review & editing. **Feliks Stobiecki:** Conceptualization, Methodology, Formal analysis, Supervision, Writing – original draft, Writing – review & editing. **Maciej Urbaniak:** Software, Formal analysis, Writing – review & editing. **Michał Matczak:** Writing – review & editing. **Gabriel David Chaves-O`Flynn:** Writing – review & editing. **Mikołaj Bilski:** Software, Writing – review & editing. **Andreas Glenz:** Methodology, Writing – review & editing. **Piotr Kuświk:** Conceptualization, Methodology, Formal analysis, Supervision, Writing – original draft, Writing – review & editing.

Declaration of Competing Interest

The authors declare that they have no known competing financial interests or personal relationships that could have appeared to influence the work reported in this paper.

Acknowledgement

The work was financed by the National Science Centre Poland under PRELUDIUM funding Grant No. UMO-2018/31/N/ST5/01810.

Appendix A. Supplementary data

Supplementary data to this article can be found online at https://doi.org/10.1016/j.jmmm.2021.168682.

References

[1] J.E. Greene, Review Article: Tracing the Recorded History of Thin-Film Sputter Deposition: From the 1800s to 2017, Journal of Vacuum Science & Technology A: Vacuum, Surfaces, and Films 35 (2017) 05C204.

[2] J. Du, X.H. Xiang, G. Landry, B. You, A. Hu, H.W. Zhao, J.Q. Xiao, Investigation of Magnetic Tunneling Junctions with Wedge-Shaped Barrier, J. Appl. Phys. 91 (2002) 8780.

[3] M. Kisielewski, A. Maziewski, M. Tekielak, A. Wawro, L.T. Baczewski, New Possibilities for Tuning Ultrathin Cobalt Film Magnetic Properties by a Noble Metal Overlayer, Phys. Rev. Lett. 89 (2002), 087203.

[4] Ł. Frąckowiak, P. Kuświk, M. Urbaniak, G.D. Chaves-O'Flynn, F. Stobiecki, Wide-Range Tuning of Interfacial Exchange Coupling between Ferromagnetic Au/Co and Ferrimagnetic Tb/Fe(Co) Multilayers, Sci Rep 8 (1) (2018), https://doi.org/10.1038/s41598-018-35042-x.

[5] Ł. Frąckowiak, P. Kuświk, G.D. Chaves-O'Flynn, M. Urbaniak, M. Matczak, P. P. Michałowski, A. Maziewski, M. Reginka, A. Ehresmann, F. Stobiecki, Magnetic Domains without Domain Walls: A Unique Effect of He + Ion Bombardment in Ferrimagnetic Tb / Co Films, Phys. Rev. Lett. 124 (2020), 047203.

[6] M. Matczak, R. Schäfer, M. Urbaniak, B. Szymański, P. Kuświk, A. Jarosz, M. Schmidt, J. Aleksiejew, S. Jurga, F. Stobiecki, Domain Wall Generated by Graded Interlayer Coupling in Co/Pt/Co Film with Perpendicular Anisotropy, Appl. Phys. Lett. 107 (1) (2015) 012404, https://doi.org/10.1063/1.4926357.

[7] Łukasz Frąckowiak, F. Stobiecki, G.D. Chaves-O'Flynn, M. Urbaniak, M. Schmidt, M. Matczak, A. Maziewski, M. Reginka, A. Ehresmann, P. Kuświk, Subsystem Domination Influence on Magnetization Reversal in Designed Magnetic Patterns in Ferrimagnetic Tb/Co Multilayers, Sci Rep 11 (1) (2021), https://doi.org/10.1038/s41598-020-80004-x.

[8] T.R. Gao, S.P. Hao, S.M. Zhou, L. Sun, Evolution of Magnetization Reversal Mechanism in Fe-Cr Alloy Films, J. Appl. Phys. 100 (7) (2006) 073909, https://doi.org/10.1063/1.2357637.

[9] J.K. Bunn, C.J. Metting, J. Hattrick-Simpers, A Semi-Empirical Model for Tilted-Gun Planar Magnetron Sputtering Accounting for Chimney Shadowing, JOM 67 (1) (2015) 154–163.

[10] W. Burgstaller, A.I. Mardare, A.W. Hassel, Copper-Zinc Thin Films Reactively Co-Sputtered from a Two-Component Sectioned Cathode: Cu-Zn Thin Film Alloys Co-Sputtered from a Two-Component Sectioned Cathode, Phys. Status Solidi A 210 (2013) 994.

[11] S.K. Suram, L. Zhou, N. Becerra-Stasiewicz, K. Kan, R.J.R. Jones, B.M. Kendrick, J. M. Gregoire, Combinatorial Thin Film Composition Mapping Using Three Dimensional Deposition Profiles, Rev. Sci. Instrum. 86 (3) (2015) 033904, https://doi.org/10.1063/1.4914466.

[12] A. Frisk, M. Ahlberg, G. Muscas, S. George, R. Johansson, W. Klysubun, P. E. Jönsson, G. Andersson, Magnetic and Structural Characterization of CoFeZr Thin Films Grown by Combinatorial Sputtering, Phys. Rev. Materials 3 (7) (2019), https://doi.org/10.1103/PhysRevMaterials.3.074403.

[13] J.K. Bunn, R.Z. Voepel, Z. Wang, E.P. Gatzke, J.A. Lauterbach, J.R. Hattrick-Simpers, Development of an Optimization Procedure for Magnetron-Sputtered Thin Films to Facilitate Combinatorial Materials Research, Ind. Eng. Chem. Res. 55 (2016) 1236.

[14] J.-M.-L. Beaujour, A.D. Kent, D.W. Abraham, J.Z. Sun, Ferromagnetic Resonance Study of Polycrystalline Fe1−xVx Alloy Thin Films, J. Appl. Phys. 103 (7) (2008) 07B519, https://doi.org/10.1063/1.2830648.

[15] B. Ruiz-Yi, T. Williams, J.K. Bunn, F. Ren, N.A. Hasan, I. Takeuchi, J. Hattrick-Simpers, A. Mehta, Phase Stabilization and Oxidation of a Continuous Composition Spread Multi-Principal Element (AlFeNiTiVZr)1−xCrx Alloy, J. Alloy. Compd. 861 (2021) 158565, https://doi.org/10.1016/j.jallcom.2020.158565.

[16] R. Collette, Y. Wu, P.D. Rack, Correlating the Optical Property Evolution in the Au-Ni Binary Thin Films: From Metastable Solid Solution to Phase Separated Alloy, J. Alloy. Compd. 793 (2019) 695.

[17] A. Marshal, K.G. Pradeep, D. Music, S. Zaefferer, P.S. De, J.M. Schneider, Combinatorial Synthesis of High Entropy Alloys: Introduction of a Novel, Single Phase, Body-Centered-Cubic FeMnCoCrAl Solid Solution, J. Alloy. Compd. 691 (2017) 683.

[18] T. Mongstad, C.C. You, A. Thogersen, J.P. Maehlen, C. Platzer-Björkman, B. C. Hauback, S.Z. Karazhanov, MgyNi1−y(Hx) Thin Films Deposited by Magnetron Co-Sputtering, J. Alloy. Compd. 527 (2012) 76–83.

[19] R.A. Dunlap, G.L. Sibley, F.N. Sy, T.D. Hatchard, Combinatorial Material Science Studies of Fe-Rich Fe–Al and Fe–Si Thin Films, J. Alloy. Compd. 470 (1-2) (2009) 27–34.

[20] H. Głowiński, F. Lisiecki, P. Kuświk, J. Dubowik, F. Stobiecki, Influence of Adjacent Layers on the Damping of Magnetization Precession in CoxFe100-x Films, J. Alloy. Compd. 785 (2019) 891–896.

[21] I. A. Makarochkin, E. V. Kudyukov, E. A. Stepanova, G. V. Kurlyandskaya, V. O. Vas'kovskiy, and A. V. Svalov, *Features of the Sperimagnetic Structure of TbCo-Based Multilayers*, in (Surabaya, Indonesia, 2020), p. 030057.

[22] P.C. Kuo, C.-M. Kuo, Magnetic Properties and Microstructure of Amorphous Co100−xTbx Thin Films, J. Appl. Phys. 84 (6) (1998) 3317–3321.

[23] J. Betz, K. Mackay, D. Givord, Magnetic and Magnetostrictive Properties of Amorphous Tb \V CoV Thin "lms, J. Magn. Magn. Mater. 8 (1999).

[24] V.O. Vas'kovskiy, O.A. Adanakova, K.G. Balymov, N.A. Kulesh, A.V. Svalov, E. A. Stepanova, Specific Features of the Formation of Atomic Magnetic Moments in Amorphous Films RE-Co (RE = La, Gd, Tb), Phys. Solid State 57 (6) (2015) 1142–1147.

[25] J. Yu, L. Liu, J. Deng, C. Zhou, H. Liu, F. Poh, J. Chen, Topological Hall Effect in Ferrimagnetic CoTb Single Layer, J. Magn. Magn. Mater. 487 (2019) 165316, https://doi.org/10.1016/j.jmmm.2019.165316.

[26] Y. Kakehashi, Modern Theory of Magnetism in Metals and Alloys, Vol. 175, Springer, Berlin Heidelberg, Berlin, Heidelberg, 2013.

[27] P. Hansen, C. Clausen, G. Much, M. Rosenkranz, K. Witter, Magnetic and Magneto-optical Properties of Rare-earth Transition-metal Alloys Containing Gd, Tb, Fe Co, Journal of Applied Physics 66 (2) (1989) 756–767.

[28] K. Ueda, M. Mann, C.-F. Pai, A.-J. Tan, G.S.D. Beach, Spin-Orbit Torques in Ta/Tb_xCo_{100-x} Ferrimagnetic Alloy Films with Bulk Perpendicular Magnetic Anisotropy, Appl. Phys. Lett. 109 (2016), 232403.

[29] A. V. Svalov, E. V. Kudyukov, K. G. Balymov, E. A. Stepanova, V. O. Vas'kovskiy, A. Larrañaga, and G. V. Kurlyandskaya, *Thickness Dependence of Magnetic Properties of Tb–Co/Ti and Tb–Co/Si Multilayers*, Phys. Metals Metallogr. **120**, 1260 (2019).

[30] B. Hebler, A. Hassdenteufel, P. Reinhardt, H. Karl, M. Albrecht, Ferrimagnetic Tb–Fe Alloy Thin Films: Composition and Thickness Dependence of Magnetic Properties and All-Optical Switching, Front. Mater. 3 (2016).

[31] M.H. Tang, Z. Zhang, S.Y. Tian, J. Wang, B. Ma, Q.Y. Jin, Interfacial Exchange Coupling and Magnetization Reversal in Perpendicular [Co/Ni]N/TbCo Composite Structures, Sci Rep 5 (2015) 10863.

[32] M. Tang, Z. Zhang, Q. Jin, Manipulation of Perpendicular Exchange Bias Effect in $[Co/Ni]_N$ /(Cu, Ta)/TbCo Multilayer Structures, AIP Adv. 5 (8) (2015) 087153, https://doi.org/10.1063/1.4929474.

[33] M. Gottwald, M. Hehn, F. Montaigne, D. Lacour, G. Lengaigne, S. Suire, S. Mangin, Magnetoresistive Effects in Perpendicularly Magnetized Tb-Co Alloy Based Thin Films and Spin Valves, J. Appl. Phys. 111 (8) (2012) 083904, https://doi.org/10.1063/1.3703666.

[34] S. Alebrand, M. Gottwald, M. Hehn, D. Steil, M. Cinchetti, D. Lacour, E.E. Fullerton, M. Aeschlimann, S. Mangin, Light-Induced Magnetization Reversal of High-Anisotropy TbCo Alloy Films, Appl. Phys. Lett. 101 (2012), 162408.

[35] R. Bläsing, T. Ma, S.-H. Yang, C. Garg, F.K. Dejene, A.T. N'Diaye, G. Chen, K. Liu, S. S.P. Parkin, Exchange Coupling Torque in Ferrimagnetic Co/Gd Bilayer Maximized near Angular Momentum Compensation Temperature, Nat Commun 9 (2018) 4984.

[36] L. Caretta, M. Mann, F. Büttner, K. Ueda, B. Pfau, C.M. Günther, P. Hessing, A. Churikova, C. Klose, M. Schneider, D. Engel, C. Marcus, D. Bono, K. Bagschik, S. Eisebitt, G.S.D. Beach, Fast Current-Driven Domain Walls and Small Skyrmions in a Compensated Ferrimagnet, Nature Nanotech 13 (12) (2018) 1154–1160.

[37] R. Tolley, T. Liu, Y. Xu, S. Le Gall, M. Gottwald, T. Hauet, M. Hehn, F. Montaigne, E.E. Fullerton, S. Mangin, Generation and Manipulation of Domain Walls Using a Thermal Gradient in a Ferrimagnetic TbCo Wire, Appl. Phys. Lett. 106 (2015), 242403.

[38] J. Yu, D. Bang, R. Mishra, R. Ramaswamy, J.H. Oh, H.-J. Park, Y. Jeong, P. Van Thach, D.-K. Lee, G. Go, S.-W. Lee, Y. Wang, S. Shi, X. Qiu, H. Awano, K.-J. Lee, H. Yang, Long Spin Coherence Length and Bulk-like Spin-Orbit Torque in Ferrimagnetic Multilayers, Nat. Mater. 18 (1) (2019) 29–34.

[39] Y. Wu, X. Zeng, Y. Guo, Q. Jia, B. Wang, J. Cao, Spin-Orbit Torque-Induced Magnetization Switching in Pt/Co–Tb/Ta Structures, Appl. Phys. Lett. 118 (2021), 022401.

[40] A. Hrabec, N.T. Nam, S. Pizzini, L. Ranno, Magnetization Reversal in Composition-Controlled Gd 1–x Co x Ferrimagnetic Films Close to Compensation Composition, Appl. Phys. Lett. 99 (2011), 052507.

[41] A. Mekonnen, M. Cormier, A.V. Kimel, A. Kirilyuk, A. Hrabec, L. Ranno, T. Rasing, Femtosecond Laser Excitation of Spin Resonances in Amorphous Ferrimagnetic Gd 1–x Co x Alloys, Phys. Rev. Lett. 107 (2011), 117202.

[42] H. Wu, J. Nance, S.A. Razavi, D. Lujan, B. Dai, Y. Liu, H. He, B. Cui, D. Wu, K. Wong, K. Sobotkiewich, X. Li, G.P. Carman, K.L. Wang, Chiral Symmetry Breaking for Deterministic Switching of Perpendicular Magnetization by Spin-Orbit Torque, Nano Lett. 21 (2021) 515.

[43] F. Richomme, J. Teillet, A. Fnidiki, P. Auric, P. Houdy, Experimental Study of the Structural and Magnetic Properties of Fe/Tb Multilayers, Phys. Rev. B 54 (1) (1996) 416–426.

[44] R.J. Gnaedinger, Some Calculations of the Thickness Distribution of Films Deposited from Large Area Sputtering Sources, Journal of Vacuum Science and Technology 6 (3) (1969) 355–362.

[45] J.J. Hanak, Compositional Determination of Rf Co-Sputtered Multicomponent Systems, Journal of Vacuum Science and Technology 8 (1) (1971) 172–175.

[46] H. Kumar, Y.K. Mishra, S. Mohapatra, D. Kabiraj, J.C. Pivin, S. Ghosh, D.K. Avasthi, Compositional Analysis of Atom Beam Co-Sputtered Metal-Silica Nanocomposites by Rutherford Backscattering Spectrometry, Nucl. Instrum. Methods Phys. Res., Sect. B 266 (8) (2008) 1511–1516.

[47] M. Knudsen, Die Molekularströmung der Gase durch Offnungen und die Effusion, Ann. Phys. 333 (1909) 999.

[48] L.I. Maissel, R. Glang, P.P. Budenstein, Handbook of Thin Film Technology, J. Electrochem. Soc. 118 (4) (1971) 114C, https://doi.org/10.1149/1.2408101.
[49] A. Ciuciulkaite, K. Mishra, M.V. Moro, I.-A. Chioar, R.M. Rowan-Robinson, S. Parchenko, A. Kleibert, B. Lindgren, G. Andersson, C.S. Davies, A. Kimel, M. Berritta, P.M. Oppeneer, A. Kirilyuk, V. Kapaklis, Magnetic and All-Optical Switching Properties of Amorphous Tb x Co 100–x Alloys, Phys. Rev. Materials 4 (2020), 104418.
[50] L. Ertl, G. Endl, H. Hoffmann, Structure and Magnetic Properties of Sputtered Tb/Co Multilayers, J. Magn. Magn. Mater. 113 (1-3) (1992) 227–237.